optica

On-chip $\chi^{(2)}$ microring optical parametric oscillator: supplementary material

ALEXANDER W. BRUCH[1], XIANWEN LIU[1], JOSHUA B. SURYA[1], CHANG-LING ZOU[2], AND HONG X. TANG[1,*]

[1]Department of Electrical Engineering, Yale University, New Haven, CT 06511, USA
[2]Department of Optics and Optics Engineering, University of Science and Technology of China, Hefei, Anhui, China
[*]Corresponding author: hong.tang@yale.edu

Published 14 October 2019

This document provides supplementary information to "On-chip $\chi^{(2)}$ microring optical parametric oscillator," https://doi.org/10.1364/OPTICA.6.001361. A detailed derivation of the optical parametric oscillation threshold and output power is presented following from the main text. A brief overview of the OPO power and conversion efficiency previously derived from input-output theory is also provided for the reader's convenience. Finally, details of the OPO measurement setup as well as the delayed self-heterodyne linewidth measurement are presented.

1. DETAILED DERIVATION OF THE OPO THRESHOLD

As previously derived in Ref .[1], the Hamiltonian for degenerate down-conversion and SHG is

$$\mathcal{H}/\hbar = \omega_a a^\dagger a + \omega_b b^\dagger b + g_0 b (a^\dagger)^2 + g_0 b^\dagger (a)^2, \tag{S1}$$

for mode a at 1550 nm and mode b at 775 nm oscillating at ω_a and ω_b, respectively. We then introduce a strong pump around mode b with the angular frequency ω_p and the pump photon number

$$\beta = \frac{\sqrt{2\kappa_{b,1}}}{-i(\omega_b - \omega_p) - \kappa_b}\sqrt{\frac{P_p}{\hbar\omega_p}} \tag{S2}$$

where $\kappa_b = \kappa_{b,0} + \kappa_{b,1}$ is the total amplitude decay rate of mode b given by intrinsic loss rate $\kappa_{b,0}$ and external coupling loss $\kappa_{b,1}$ and is related to optical Q by $\kappa_b = \frac{\omega_b}{2Q_b}$. Applying a mean field approximation in the rotating frame of ω_a, the effective Hamiltonian from Eq. (S1) of the probe field a is reduced to

$$\mathcal{H}_{eff}/\hbar = \delta_a a^\dagger a + g_0\beta((a^\dagger)^2 + a^2) \tag{S3}$$

where $\delta_a = \omega_a - \omega_p/2$ represents the detuning of the signal (idler) mode frequency from the downconverted pump frequency.

Due to the coupling ports and intrinsic losses, we write the system Langevin equations as

$$\frac{d}{dt}a = (-i\delta_a - \kappa_a)a - ig_0\beta a^\dagger - i\sqrt{2\kappa_{a,0}}a_{in} - i\sqrt{2\kappa_{a,1}}a_{in} \tag{S4}$$

$$\frac{d}{dt}a^\dagger = (i\delta_a - \kappa_a)a^\dagger - ig_0\beta a + i\sqrt{2\kappa_{a,0}}a^\dagger_{in} + i\sqrt{2\kappa_{a,1}}a^\dagger_{in} \tag{S5}$$

where a_{in} and $a^\dagger_{in}$ refer to the input at mode a due to vacuum noise. Introducing the Fourier Transform of operators

$$\mathcal{O}(\omega) = \int dt \mathcal{O}(t) e^{i\omega t}, \tag{S6}$$

$$\mathcal{O}^\dagger(-\omega) = \int dt \mathcal{O}^\dagger(t) e^{i\omega t}, \tag{S7}$$

we obtain

$$-i\omega a_= (-i\delta_a - \kappa_a)a - ig_0\beta a^\dagger - i\sqrt{2\kappa_{a,0}}a_{in} - i\sqrt{2\kappa_{a,1}}a_{in}, \tag{S8}$$

$$-i\omega a^\dagger = (i\delta_a - \kappa_a)a^\dagger + ig_0\beta a + i\sqrt{2\kappa_{a,0}}a^\dagger_{in} + i\sqrt{2\kappa_{a,1}}a^\dagger_{in}, \tag{S9}$$

where the $o^\dagger$ terms correspond to the $-\omega$ frequency.

The cavity field is then solved as

$$a = \frac{-\chi'_a(-i\sqrt{2\kappa_{a,0}}a_{in} - i\sqrt{2\kappa_{a,1}}a_{in}) - ic(i\sqrt{2\kappa_{a,0}}a^\dagger_{in} + i\sqrt{2\kappa_{a,1}}a^\dagger_{in})}{\chi_a\chi'_a - |c^2|} \tag{S10}$$

where

$$c = \frac{g_0\beta}{\kappa_a}, \tag{S11}$$

$$\chi_a = \frac{-i(\delta_a - \omega)}{\kappa_a} - 1, \tag{S12}$$

$$\chi_a' = \frac{-i(\delta_a + \omega)}{\kappa_a} - 1. \tag{S13}$$

The top term in Eq. (S10) refers to the input from vacuum noise and is particularly important for spontaneous parametric down-conversion experiments such as Ref. [1]. For the OPO case however, we have oscillation at a without external laser input, giving the expression

$$\chi_a\chi_a' - |c^2| \approx 0, \tag{S14}$$

yeilding the threshold condition

$$g_0^2\beta^2 = \kappa_a^2, \tag{S15}$$

shown in Eq. (4) in the main text. Expanding out terms and assuming critical coupling as well as the pump on resonance ($\omega_p = \omega_b$) we obtain

$$P_{th} = \frac{\hbar\omega_b}{g_0^2}\kappa_{a,0}^2\kappa_{b,0} = \frac{\hbar\omega_b^4}{32g_0^2}\frac{1}{Q_{a,0}^2 Q_{b,0}}. \tag{S16}$$

2. OPO POWER ABOVE THRESHOLD

A. Degenerate OPO

In the previous section, we made the non-depletion approximation for for OPO below threshold. When the pump exceeds the threshold, however, $|a|^*$ will be amplified until saturation. Here, we solve the OPO output power without the backaction approximation, but neglect the quantum noise.

From Eq. (S1), we have

$$\dot{a} = (-i\delta_a - \kappa_a)a - i2g_0ba^* \tag{S17}$$

$$\dot{b} = (-i\delta_b - \kappa_b)b - ig_0a^2 - i\sqrt{2\kappa_{b1}}b_{in} \tag{S18}$$

where the input has frequency ω_p, the pump detuning is given by $\delta_b = \omega_b - \omega_p$, and $b_{in} = \sqrt{\frac{P_p}{\hbar\omega_p}}$ is the input photon number at mode b from the pump. In the steady state of OPO above threshold, we have

$$\dot{a} = 0 \tag{S19}$$

$$\dot{b} = 0 \tag{S20}$$

such that

$$a = \frac{i2g_0b}{-i\delta_a - \kappa_a}a^*. \tag{S21}$$

Let $a = |a|e^{i\theta}$, then $b = \frac{-i\delta_a-\kappa_a}{i2g_0}e^{i2\theta}$. Substituting it into Eq. S18, we have

$$\frac{(-i\delta_a - \kappa_a)(-i\delta_b - \kappa_b)}{i2g_0}e^{i2\theta} - ig_0|a|^2e^{i2\theta} - i\sqrt{2\kappa_{b,1}}b_{in} = 0 \tag{S22}$$

such that

$$\frac{(-i\delta_a - \kappa_a)(-i\delta_b - \kappa_b)}{2g_0^2} + |a|^2 + \frac{\sqrt{2\kappa_{b1}}}{g_0}e^{-i2\theta}b_{in} = 0. \tag{S23}$$

If the real and imaginary parts of Eq. (S23) both vanish in the steady state, then

$$\frac{i\delta_a\kappa_b + i\delta_b\kappa_a}{2g_0^2} - i\frac{\sqrt{2\kappa_{b1}}}{g_0}\sin(2\theta)b_{in} = 0, \tag{S24}$$

$$\sin(2\theta) = \frac{\delta_a\kappa_b + \delta_b\kappa_a}{2g_0\sqrt{2\kappa_{b1}}b_{in}}, \tag{S25}$$

and

$$\frac{\kappa_a\kappa_b - \delta_a\delta_b}{2g_0^2} + |a|^2 + \frac{\sqrt{2\kappa_{b1}}}{g_0}b_{in}\cos(2\theta) = 0 \tag{S26}$$

$$|a|^2 = \frac{\sqrt{2\kappa_{b1}}}{g_0}b_{in}\sqrt{1 - \left(\frac{\delta_a\kappa_b + \delta_b\kappa_a}{2g_0\sqrt{2\kappa_{b1}}b_{in}}\right)^2} - \frac{\kappa_a\kappa_b\delta_a\delta_b}{2g_0^2}. \tag{S27}$$

Equation (S27) only has a solution when the right hand side is greater than zero. For the ideal case of $\delta_a = \delta_b = 0$, then

$$|a|^2 = \frac{\sqrt{2\kappa_{b1}}}{g_0}b_{in} - \frac{\kappa_a\kappa_b}{2g_0^2}. \tag{S28}$$

We note that the above equation can be used to verify the OPO threshold when $\sqrt{2\kappa_{b1}}b_{in} \geq \frac{\kappa_a\kappa_b}{2g_0}$ in the form

$$\sqrt{2\kappa_{b1}}\sqrt{\frac{P_{th}}{\hbar\omega_b}} = \frac{\kappa_a\kappa_b}{2g_0}, \tag{S29}$$

then we obtain the threshold

$$P_{th} = \frac{\kappa_a^2\kappa_b^2}{8\kappa_{b1}g_0^2}\hbar\omega_b. \tag{S30}$$

If we define the single-photon cooperativity as

$$C_0 = \frac{g_0^2}{\kappa_a\kappa_b} = \frac{1}{\frac{P_{th}}{\hbar\omega_b}\frac{8\kappa_{b1}}{\kappa_b}\frac{1}{\kappa_a}}, \tag{S31}$$

Eq. (S28) can be re-written as

$$|a|^2 = \frac{1}{2C_0}(\sqrt{P_b/P_{th}} - 1). \tag{S32}$$

Therefore, the IR OPO output is

$$P_{s+i} = 2\kappa_{a1}\hbar\omega_a|a|^2 \tag{S33}$$

$$= 2\kappa_{a1}\hbar\omega_a\frac{P_{th}}{\hbar\omega_b}\frac{4\kappa_{b1}}{\kappa_b}\frac{1}{\kappa_a}(\sqrt{P_b/Pth} - 1) \tag{S34}$$

$$= 4\frac{\kappa_{a1}}{\kappa_a}\frac{\kappa_{b1}}{\kappa_b}P_{th}(\sqrt{P_b/P_{th}} - 1). \tag{S35}$$

B. Non-degenerate OPO

The total Hamiltonian for non-degenerate downconversion and DFG can be written as [1]

$$\mathcal{H}/\hbar = \omega_a a^\dagger a + \omega_c c^\dagger c + \omega_b b^\dagger b + 2g_0bc^\dagger a^\dagger + 2g_0b^\dagger ca + \sqrt{2\kappa_{b1}}(b^\dagger b_{in}e^{-i\omega_p t} + b_{in}^\dagger e^{i\omega_p t}b), \tag{S36}$$

by accounting that three-wave mixing coupling strength in the non-degenerate case is twice that of the degenerate case. Here, modes a and c near 1550 nm and mode b at 775 nm oscillating at ω_a, ω_c, and ω_b, respectively. Assuming all modes on resonance

and phase-matching such that $\omega_a + \omega_c = \omega_b$ and $\omega_b = \omega_p$, we find the steady-state relations

$$\dot{a} = -\kappa_a a - i2g_0 bc^* = 0, \tag{S37}$$
$$\dot{c} = -\kappa_c c - i2g_0 ba^* = 0, \tag{S38}$$
$$\dot{b} = -\kappa_b b - i2g_0 ac - i\sqrt{2\kappa_{b1} b_{in}} = 0, \tag{S39}$$

yielding

$$\kappa_a a = -i2g_0 bc^*, \tag{S40}$$
$$\kappa_c c = -i2g_0 b\frac{ig_0 b^*}{\kappa_a} c, \tag{S41}$$
$$\kappa_a \kappa_c ac = -4g_0^2 b^2 a^* c^*, \tag{S42}$$

from which we may note $|b|^2 = \frac{\kappa_a \kappa_c}{4g_0^2}$.

Setting the real part of Eq. (S42) to zero, we find

$$\kappa_a a(i2g_0 ba^*) = \kappa_c c(i2g_0 bc^*), \tag{S43}$$
$$\kappa_a |a|^2 = \kappa_c |c|^2. \tag{S44}$$

Similarly, for the imaginary part of Eq. (S42), we find

$$\pm i\kappa_b \frac{\sqrt{\kappa_a \kappa_c}}{4g_0^2} - i2g_0 \frac{-i2g_0}{\kappa_a}|c|^2(\pm i\frac{\kappa_a \kappa_c}{4g_0^2}) - i\sqrt{2\kappa_{b1}} b_{in} = 0, \tag{S45}$$
$$\frac{-4g_0^2}{\kappa_a}|c|^2 = \kappa_b - \frac{\sqrt{2\kappa_{b1}} b_{in} 2g_0}{\kappa_a \kappa_c}, \tag{S46}$$
$$|c|^2 = \frac{\sqrt{2\kappa_{b1}}}{2g_0\sqrt{\kappa_c/\kappa_a}} b_{in} - \frac{\kappa_a \kappa_b}{4g_0^2}. \tag{S47}$$

From the above relations, we can verify the non-degenerate OPO threshold, noting that Eq. (S47) only has a solution when the right hand side is greater than zero, yielding

$$\frac{\sqrt{2\kappa_{b1}}}{2g_0\sqrt{\kappa_c/\kappa_a}}\sqrt{\frac{P_{th}}{\hbar\omega_b}} = \frac{\kappa_a \kappa_b}{4g_0^2}, \tag{S48}$$
$$P_{th} = \frac{\kappa_a \kappa_c \kappa_b^2}{8g_0^2 \kappa_{b1}} \hbar\omega_b, \tag{S49}$$

which is equivalent to that derived above.

Defining the single-photon cooperativity for modes a and c as

$$C_{0,ac} = \frac{g_0^2}{\kappa_{a,c}\kappa_b} = \frac{1}{\frac{P_{th}}{\hbar\omega_b}\frac{8\kappa_{b1}}{\kappa_b}\frac{1}{\kappa_{a,c}}} \tag{S50}$$

we may re-write Eq. (S47) as

$$|c|^2 = \frac{1}{4C_{0,ac}}(\sqrt{P_b/P_{th}} - 1) \tag{S51}$$

for mode c and similarly

$$|a|^2 = \frac{1}{4C_{0,ac}}(\sqrt{P_b/P_{th}} - 1) \tag{S52}$$

for mode a.

We then solve the steady-state OPO output power as

$$P_{s+i} = 2\kappa_{a1}|a|^2\hbar\omega_a + 2\kappa_{c1}|c|^2\hbar\omega_c \tag{S53}$$
$$\approx \left(\frac{2\kappa_{a1}}{\kappa_a} + \frac{2\kappa_{c1}}{\kappa_c}\right)\frac{\hbar\omega_b}{2}\frac{\kappa_a\kappa_c\kappa_b}{4g_0^2}(\sqrt{P_b/P_{th}} - 1) \tag{S54}$$
$$\approx \left(\frac{2\kappa_{a1}}{\kappa_a} + \frac{2\kappa_{c1}}{\kappa_c}\right)\frac{\kappa_{b1}}{\kappa_b}P_{th}(\sqrt{P_b/P_{th}} - 1). \tag{S55}$$

If we assume that modes a and c are sufficiently close such that $\omega_c \approx \omega_c$, $\kappa_c \approx \kappa_a$, and $\kappa_{c1} \approx \kappa_{a1}$, then Eq. S55 simplifies to

$$P_{s+i} \approx 4\frac{\kappa_{a1}}{\kappa_a}\frac{\kappa_{b1}}{\kappa_b}P_{th}(\sqrt{P_b/P_{th}} - 1). \tag{S56}$$

When we have critical coupling for both visible and telecom bands,

$$P_{s+i} \approx P_{th}(\sqrt{P_b/P_{th}} - 1). \tag{S57}$$

C. Discussion

From the Eqs. (S35) and (S55), we have the energy conversion efficiency

$$\eta_{s+i} = 4\frac{\kappa_{a1}}{\kappa_a}\frac{\kappa_{b1}}{\kappa_b}(\sqrt{P_{th}/P_b} - P_{th}/P_b). \tag{S58}$$

This equation has a few notable features. First, we note that the energy conversion efficiency η_{s+i} scales roughly as $\sqrt{P_b/P_{th}}$; unlike in the SHG case the OPO efficiency cannot be increased by increasing the pump power to saturation. Instead, Eq. (S58) has a maximum specifically at $P_b = 4P_{th}$. Second, we find that by inserting $P_b = 4P_{th}$ in to Eq. (S58) we achieve a maximum efficiency of 25% in the critically coupled case. Finally, this maximum efficiency is determined by the extraction factors $\frac{\kappa_{a,1}}{\kappa_a}$ and $\frac{\kappa_{b,1}}{\kappa_b}$ in Eqs. (S35) and (S55); $\eta_{s+i,max}$ is increased and decreased by over- and undercoupling, respectively. This finding is of fundamental importance to designing an OPO laser. We note that over-coupling helps to increase the OPO efficiency, however undercoupling is usually preferable to decrease the OPO threshold. The design of an OPO laser must balance these competing goals; a high conversion effciency suffers from a high OPO threshold, and vice-versa.

3. COMPARISON TO INPUT-OUTPUT THEORY

The reader is also encouraged to refer to Refs. [2, 3] for a thorough derivation of the OPO threshold, OPO power, and conversion efficiency from input-output theory. Here, we will summarize the equations used therein to establish their equivalence to those derived above.

A. OPO Threshold

Using the formalism defined in Ref. [1], the term g_0^2 can be expanded as

$$g_0^2 = \frac{\hbar\omega_b^3 {\chi^{(2)}}^2}{8\pi\epsilon_0 R n_{\text{eff}}^6}\xi^2 \tag{S59}$$

where n_{eff} is the effective index of the phase matched pump, signal, and idler modes, and ξ is the effective mode overlap factor. The expanded form of g_0 is then inserted into Eq. (S16) to find

$$P_{th} = \frac{\omega_b \pi\epsilon_0 n_{\text{eff}}^6}{4{\chi^{(2)}}^2}\frac{1}{Q_a^2 Q_b}\frac{R}{\xi^2}. \tag{S60}$$

After relating R/ξ^2 to effective mode volume V_{eff}, Eq. (S60) can be related to the expression derived in Ref. [3]

$$P_{th} = \frac{\pi\nu_b\epsilon_0 n_{eff}^6}{16d^2}\frac{1}{Q_a^2 Q_b}V_{eff}. \tag{S61}$$

An examination of these equations yields useful scaling relations of the OPO threshold. Notably, the threshold decreases when moving to longer pump wavelengths, reducing the optical loss (particularly at the signal/idler wavelengths), or using a material

with a large $\chi^{(2)}$ value. The threshold increases with larger mode volume and/or poor mode overlap; our AlN microresonators are able to achieve OPO lasing with relatively small optical Q factors compared to bulk resonators due to their significantly reduced mode volume and high mode overlap.

B. OPO Power and Efficiency

We begin by adopting the conventions from Ref. [3], introducing the coupling parameter $r = Q_0/Q_1$ such that $r < 1$ represents undercoupling, $r > 1$ represents overcoupling, and $r = 1$ is the critically-coupled case. The generated signal power is derived as

$$P_s = 4(\sqrt{P_b/P_{th}} - 1)P_{th}\frac{\lambda_b}{\lambda_s(r_b^{-1}+1)^2(r_{si}^{-1}+1)^2} \quad \text{(S62)}$$

$$= \frac{2}{R}(\sqrt{P_b/P_{th}} - 1)P_{th} \quad \text{(S63)}$$

and similarly for the idler. Assuming $\lambda_s \approx \lambda_b/2$ for simplicity. The total signal and idler power is simply twice this quantity, then

$$P_{s+i} = \frac{16}{(r_b^{-1}+1)^2(r_{si}^{-1}+1)^2}P_{th}(\sqrt{P_p/P_{th}} - 1). \quad \text{(S64)}$$

When we have critical coupling for both visible and telecom bands,

$$P_{s+i} \approx P_{th}(\sqrt{P_b/P_{th}} - 1), \quad \text{(S65)}$$

which agrees with the derivations in previous section.

4. OPO MEASUREMENT SETUP

The data presented in Fig. 3(a-b) in the main text was collected using the setup shown in Fig. S1. The pump light used to excite the OPO is sourced by a Ti:Sapphire laser (M2 SolsTiS, 700−1000 nm) and a variable neutral density filter (ND) is employed to adjust the input power delivered to the chip. The polarization of the incident light is then selected for the TM mode by a half-wave plate ($\lambda/2$) before it is focused onto the AlN waveguide via an aspheric lens (L1). The AlN chip is placed upon an external heater for fine tuning the temperature to the dually-resonant condition. Since the extracted signal and idler photons in the waveguide mainly propagate towards the input facet (solid arrows in Fig. S1), a dichroic mirror (M1, Thorlabs DMSP950T) is placed in front of the aspheric lens to reflect the backward-traveling infrared OPO light into an integrating sphere detector (Thorlabs S144C, PD1). The transmitted visible and scattered infrared light is then collected by a lensed fiber (LF) and then separated via an off-chip wavelength division multiplexer (WDM). The visible light is collected into a photodetector for monitoring the transmission while the scattered infrared light is diverted towards an optical spectrum analyzer (AQ 6315E) and a high-sensitivity infrared photodetector (PD2).

5. SELF-HETERODYNE LINEWIDTH MEASUREMENT

Several experimental techniques exist to measure the linewidth of a narrowband laser and are usually cross-correlation (involving an auxillary laser) or autocorrelation (no auxillary laser). Examples of the former case include heterodyne spectroscopy, where the auxillary laser is swept over the probe laser, and heterodyne beating, where the auxillary laser beats with the probe laser and the linewidth of the resulting beat note is measured in the RF domain [4]. Such measurement schemes are relatively

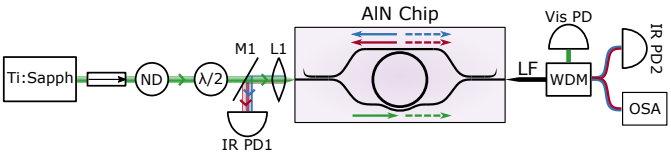

Fig. S1. Schematic of the experimental set-up for OPO characterization. Note that the OPO light in the waveguide (upper solid arrows) mainly propagates towards the input facet while approximately 10% (upper dashed arrows) is scattered towards the output chip facet due to residual waveguide roughness and/or scattering from the bus waveguides. Descriptions of each component are given in the text.

simple to implement, however the retrieved linewidth is ultimately limited by the linewdith of the auxillary laser.

Here we apply an autocorrelation technique – the self-heterodyne scheme, where a laser is split and one portion is delayed (usually by an optical fiber) and then re-combined with the original beam in a Mach-Zhender interfometer scheme [5]. The reference (non-delayed) arm is typically frequency shifted by an acousto-optic modulator (AOM) to a covenient frequency in the RF domain; a beat note will arise at the AOM drive frequency if the recombined beams retain sufficient coherence after delay in the optical fiber. The laser linewidth can be directly retrieved from the linewidth of the RF beatnote, however this technique is known to be particularly sensitive to intrinsic laser noise such as $1/f$ and flicker noise [6].

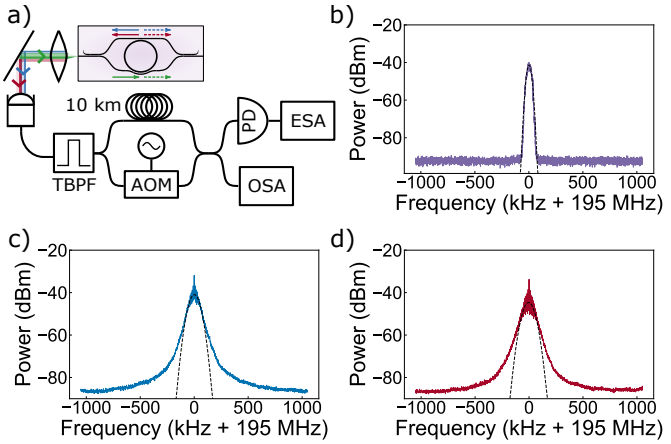

Fig. S2. (a) Experimental setup for laser linewidth measurement. Details on each component are given in the main text. (b) Retrieved RF beatnote from the self-heterdyne measurement in the degenerate lasing case. A gaussian fit (dashed black line) is applied to the spectrum to retrieve the linewidth. RF beat notes of the (c) signal and (d) idler are also retrieved and a gaussian fit is applied as before.

The experimental setup used to assess the laser linewidth is shown in Fig. S2(a). The setup is identical to Fig. S1, except that we have replaced PD1 with an infrared collimator to collect the OPO light into a fiber. The light is then sent to an optical tunable bandpass filter (TBPF) set for either the signal, idler, or degenerate wavelengths to remove other spectral components from the measurement. The light is then split into two branches. One branch is sent to a 10.56 km fiber delay line, while the reference arm is sent to an AOM (Gooch & Housego Fiber-Q)

driven at 195 MHz. The two signals then recombine and interfere on a photodetector (New Focus 1611) and the resulting beat note is aquired on an electrical spectrum analyzer (ESA, Signal Hound USB-SA124B). We also monitor the filtered laser line on an OSA to ensure filter alignment during the measurement. All split ratios are approximately 50:50. We choose a fiber length of 10.56 km as it is longer than the coherence length of the pump laser which is specified as <50 kHz, or 2.3 km SMF at 1550 nm.

The retrieved RF beat notes and a gaussian fit of their respective spectra are shown in Fig. S2 (b-d). The degenerate case results in an almost perfect gaussian distribution with a measured linewidth of 34 kHz and is likely limited by the linewidth of the pump laser. A broader beat-note of 85 kHz is observed in the non-degenerate signal and idler which deviates significantly from the gaussian-like behavior at frequencies beyond $\pm$300kHz. Here, the linewidth begins to follow a $1/f$-like shape due to additional phase noise in the non-degenerate phasematching condition [6]. An in-depth investigation of this behavior using more rigorous stability measurements such as the three-cornered hat method [7, 8] is needed to confirm the origin on this noise and is beyond the scope of this work.

REFERENCES

1. X. Guo, C.-l. Zou, C. Schuck, H. Jung, R. Cheng, and H. X. Tang, "Parametric down-conversion photon-pair source on a nanophotonic chip," Light. Sci. & Appl. **6**, e16249 (2016).
2. B. Sturman and I. Breunig, "Generic description of second-order nonlinear phenomena in whispering-gallery resonators," J. Opt. Soc. Am. B **28**, 2465 (2011).
3. I. Breunig, "Three-wave mixing in whispering gallery resonators," Laser & Photonics Rev. **10**, 569–587 (2016).
4. Jihong Geng, S. Staines, Zuolan Wang, Jie Zong, M. Blake, and Shibin Jiang, "Highly stable low-noise Brillouin fiber laser with ultranarrow spectral linewidth," IEEE Photonics Technol. Lett. **18**, 1813–1815 (2006).
5. A. Canagasabey, A. Michie, J. Canning, J. Holdsworth, S. Fleming, H.-C. Wang, M. L. Åslund, A. Canagasabey, A. Michie, J. Canning, J. Holdsworth, S. Fleming, H.-C. Wang, and M. L. Åslund, "A Comparison of Delayed Self-Heterodyne Interference Measurement of Laser Linewidth Using Mach-Zehnder and Michelson Interferometers," Sensors. **11**, 9233–9241 (2011).
6. W. Ma, B. Xiong, C. Sun, X. Ke, Z. Hao, L. Wang, J. Wang, Y. Han, H. Li, and Y. Luo, "Laser frequency noise characterization by self-heterodyne with both long and short delay," Appl. Opt. **58**, 3555 (2019).
7. E. de Carlos López and J. L. Romero, "Frequency stability estimation of semiconductor lasers using the three-cornered hat method," in *Fifth Symposium Optics in Industry*, , vol. 6046 (International Society for Optics and Photonics, 2006), p. 604621.
8. M. C. Collodo, F. Sedlmeir, B. Sprenger, S. Svitlov, L. J. Wang, and H. G. L. Schwefel, "Sub-kHz lasing of a CaF_2 whispering gallery mode resonator stabilized fiber ring laser," Opt. Express **22**, 19277 (2014).